applied sciences

MDPI

Article

Synthesis, Characterization, and Antibacterial Activity of Graphene Oxide/Zinc Hydroxide Nanocomposites

Jo Ann Sanchez [1], Luis Materon [2], Jason G. Parsons [3] and Mataz Alcoutlabi [1,*]

[1] Mechanical Engineering Department, University of Texas Rio Grande Valley, Edinburg, TX 78539, USA; joann.sanchez01@utrgv.edu
[2] Department of Biology, University of Texas, Rio Grande Valley, Edinburg, TX 78539, USA
[3] School of Earth, Environmental, and Marine Sciences, University of Texas, Rio Grande Valley, 1 W University Blvd., Brownsville, TX 78521, USA; jason.parsons@utrgv.edu
* Correspondence: mataz.alcoutlabi@utrgv.edu; Tel.: +956-665-8945

Abstract: Graphene and graphene oxide have shown good antibacterial activity against different bacterial species due to their unique physicochemical properties. Graphene oxide (GO) has been widely used to load metallic and metal oxide nanoparticles (NPs) to minimize their surface energy during processing and preparation, hence reducing their aggregation. In this work, GO was effectively synthesized and coated with different concentrations of zinc hydroxide Zn (OH)x using the precipitation method to prepare a GO/Zn (OH)x hybrid composite. The Zn (OH)x NPs and GO/Zn (OH)x nanocomposites were synthesized and characterized using various methods such as scanning electron microscopy (SEM), X-ray diffraction (XRD), and X-ray photoelectron spectroscopy (XPS). Coating GO with Zn (OH)x NPs resulted in improved aggregation of Zn (OH)x NPs as well as enhanced antibacterial activity of GO against Gram-positive and Gram-negative bacteria. Additionally, the effect of Zn (OH)x coating on the antibacterial properties of the GO/Zn (OH)x composite was systematically investigated. The synergistic effects of GO and Zn (OH)x NPs resulted in enhanced antibacterial properties of the composites compared to the pristine GO material. In addition, increasing the Zn (OH)x wt. % concentration led to an increased inhibition zone of the GO/Zn (H)x composite against Bacillus megaterium and E. coli bacteria.

Keywords: graphene oxide; zinc hydroxide; antibacterial activity; *E. coli*; nanoparticles

Citation: Sanchez, J.A.; Materon, L.; Parsons, J.G.; Alcoutlabi, M. Synthesis, Characterization, and Antibacterial Activity of Graphene Oxide/Zinc Hydroxide Nanocomposites. *Appl. Sci.* **2024**, *14*, 6274. https://doi.org/10.3390/app14146274

Academic Editor: Jorge Bañuelos Prieto

Received: 8 June 2024
Revised: 8 July 2024
Accepted: 12 July 2024
Published: 18 July 2024

1. Introduction

There has been grown interest in the use of nanomaterials as antibacterial agents against different bacterial species with the aim of treating and preventing bacterial infections [1,2]. The unique chemical and physical characteristics of nonmetals can overcome antibiotic resistance by initiating a leakage in the bacterial membrane cells [2,3]. Metals, metal oxide NPs, and metallic NPS/graphene- or graphene oxide (GO)-based nanomaterials have been widely tested against Gram-positive and Gram-negative bacteria due to their synergetic effects [4–7].

Carbon-based nanomaterials have been used in many applications, such as renewable energy alternatives, energy storage, environmental sensors, pollution preventative material, and as antimicrobial agents [8–12]. Graphene is a single layer of graphite, sp^2-bonded carbon, and a 2-dimensional material that can be molded into various structures with unique physical, chemical, and mechanical properties [13–16]. In fact, graphene can be chemically modified, and its physical and chemical properties can change [13,14]. Moreover, graphene, graphene oxide, and reduced graphene oxide have all shown some antibacterial resistance [4,17,18]. The antibacterial properties of graphene are improved even further by oxidation, which results in graphene oxide, a product that includes significant oxygen functional groups in its structure. These functional groups include carbonyl, carboxyl, and hydroxyl, which make graphene oxide hydrophilic and negatively charged. The fact that GO is able to form stable solutions in water results in GO solutions for versatile

applications [19]. GO is also easily processed, low-cost, and mass-produced. Recently, graphene oxide has shown strong antibacterial properties [20,21]. In fact, the presence of oxygen functional groups in its structure makes GO excellent for antibacterial applications, drug delivery, and decontamination. The cytotoxicity and good antibacterial properties of graphene and GO can be attributed to different mechanisms, including oxidative stress generated by charge transfer and reactive oxygen species (ROS), membrane stress caused by the direct contact between the graphene (or GO) sharp edge and the bacterial membrane, wrapping or trapping the bacteria cell membrane (by GO sheets), basal plane destruction (defects in graphene), and photothermal effects [4]. Graphene and graphene oxide can also chemically react with bacteria via oxidative stress and charge transfer mechanisms [18]. Oxidative stress is the most important factor in determining the antibacterial activity or toxicity of graphene and GO [22,23]. In fact, the ROS of GO can damage the DNA and cause mitochondrial dysfunction, hence leading to the inhibition of bacteria [24–26]. The production of ROS leads to severe oxidative stress that can disrupt the cell by causing RNA/DNA damage, disruption of protein production, and inhibition of enzymes [27–29]. There have also been reports attributing the strong antibacterial activity of GO to membrane stresses caused by the sharp, thin edges of the GO nanosheets [7,30]. The destruction of *E-coli* cells by direct contact with GO has already been reported in the literature [26].

Moreover, various metals and metal oxides such as Ag, Cu, TiO, CuO, and ZnO have been reported to inhibit bacteria [27,31–34]. Zinc and Zn-based nanomaterials have been commonly used for commercial applications such as cosmetics, sunscreen, semiconductors, and food preservation [35–37]. The cytotoxicity and good antibacterial properties of metals and metal oxides are attributed to the fact that they can inactivate proteins and enzymes in bacteria via the binding of metal ions^{+} on the cell surface, forming reactive oxygen species (ROS) and/or interfering with nutrient absorption and the cell structure [5,38]. In fact, the interaction between metallic ions and bacterial cell membranes can spoil the metabolic activity of the bacterium by inactivating its cell [33,39]. The results reported in the literature showed that the antibacterial activity of metal oxides against bacterial species was attributed to the releases of toxic metallic ions that can kill the bacteria as well as to the oxidative stress, damage of the cell membrane, inhibition of enzymes, lipid peroxidation, and proteolysis [40].

Metal oxides such as ZnO NPs have been widely used in different applications and received significant attention owing to their toxicity and potential risks to human health and the environment [41–43]. However, the exact mechanism for its antimicrobial properties is not yet fully understood. The development of ROS species, as well as electrostatic forces in ZnO, can disrupt the cell membrane and hence inhibit a large variety of bacteria [27,44,45]. Consequently, the synthesis of more complex structures using ZnO and Zn $(OH)_x$ has been a topic of interest for improving their properties. In fact, zinc oxide (ZnO) is a white powder used in sunscreens, rubber products, and paints, while zinc hydroxide ($Zn(OH)_2$) is a white precipitate used in chemical reactions to form salts and water. Above all, hybrid structures incorporating ZnO NPs and carbon are being heavily studied. For example, Zhoe et al. successfully reported the synthesis of ZnO-rGO nanorods using zinc nitrate precursor, which resulted in a hybrid material that exhibited a high performance of photocatalytic degradation [46]. Other studies indicated that ZnO could effectively be combined with GO to prepare nanocomposites with stable nanostructures such as nanorods, nano walls, sheets, and nanoparticles [47–49]. Hydroxides have been widely used in different applications, such as in solar cells [50] and supercapacitors [51]; however, the use of zinc hydroxide ($Zn(OH_2)$) in biological and health science applications is relatively novel. Interestingly, (Zn (OH_2)) exhibits good antibacterial and excellent physical properties, biocompatibility, and biodegradability. The results reported in the literature showed that $Zn(OH)_2$ exhibited good antibacterial activity against Gram-positive bacterial strains. On the other hand, layered zinc hydroxide has been briefly investigated for drug delivery-related applications. The results reported by Nabipour et al. showed excellent antibacterial properties of layered

zinc hydroxide, intercalated with amoxicillin trihydrate, against Gram-positive bacteria *Staphylococcus aureus*, *Klebsiella pneumonia*, and Gram-negative *Escherichia coli* [52].

In this work, graphene oxide was effectively synthesized and coated with different concentrations of zinc hydroxide to prepare a GO/Zn $(OH)_x$ hybrid composite using a simple precipitation method/titration. In fact, there was no physical coating of Zn (OH)x on GO substrates, such as when using the sputter coating method or other processes. The coating of GO with different concentrations of Zn (OH)x NPs was performed using the precipitation synthesis method used in the present work. The effect of Zn $(OH)_x$ coating on the antibacterial properties of the GO/Zn$(OH)_x$ composites against *bacillus megaterium* and *E. coli* bacteria was systematically investigated. It is anticipated that the Zn $(OH)_x$ NPs/GO nanocomposite may show enhanced antibacterial activity compared to Zn $(OH)_x$ NPs or to the pristine GO.

The main reason for using these bacteria in the present study is to observe the difference in behavior between the two different bacteria using a Gram-positive *Bacillus* species that produces spores that belong to the same genus of serious pathogens to humans and a Gram-negative *Enterobacteriaceae*/*Escherichia coli* as a standard coliform pathogen. There is a structural difference in the cell wall of both bacteria tested. In fact, the focus of the current study is not only on the antibacterial activity of GO and GO/Zb(OH)x nanocomposite but also on their morphology and structural characterization. One of the main focuses of the present manuscript is the synthesis of Zb(OH)x, which is novel. To the best of the authors' knowledge, there is not sufficient work reported on the antibacterial activity of GO/Zb(OH)x nanocomposite against different bacterial species.

2. Experimental Section

2.1. Materials

Graphite powder, zinc nitrate tetrahydrate, and sodium hydroxide were purchased from Fisher Scientific (Hampton, NH, USA). Potassium permanganate ($KMnO_4$) was purchased from ACROS. Sulfuric acid (H_2SO_4), hydrogen peroxide (H_2O_2), hydrochloric acid (HCl), and sodium nitrate ($NaNO_3$) were obtained from Sigma-Aldrich (St. Louis, MO, USA). Zinc nitrate tetrahydrate was purchased from was purchased from MP Biomedicals (Irvine, CA, USA).

2.2. Synthesis of GO

Graphene oxide was synthesized using a modified Hummer's Method. A mixture of graphite powder (3 g), sodium nitrate (1.5 g), and sulfuric acid 969 mL was prepared and chilled in an ice bath until it reached a temperature of 4 °C while being stirred magnetically [53]. After the mixture was adequately chilled, 9 g of potassium permanganate was added at a rate of 0.5 g/min. Once the $KMnO_4$ was completely added, 138 mL of deionized water was added dropwise while ensuring the temperature did not go over 60 °C. Next, the solution was heated to 98 °C for 15 min and allowed to chill to room temperature. Afterward, hydrogen peroxide (3 mL) and 400 mL of deionized water were added to the mixture. Finally, the solution was vacuum-filtered and washed twice with deionized water and once with acetone. The final product was dried in a furnace oven for 24 h at a temperature of 90 °C.

2.3. Synthesis of GO/ZnOH Composite

GO (1 g) was uniformly dispersed in 1 L of deionized water by magnetic stirring for 30 min. Zinc nitrate tetrahydrate was then added to the GO solution. A 0.1 M solution of NaOH was also prepared by dissolving NaOH pellets in 100 mL of DI. The 0.1 M NaOH solution was then added dropwise using a pump. After the titration was finished, the solution was heated to 98 °C for 2 h. The solution was magnetically stirred throughout the entire process. Finally, the solution was centrifuged, washed twice with DI, and washed once with acetone. The precipitate was left to dry overnight at 80 °C in a furnace oven. The amount of Zn $(NO_3)_2$ and NaOH was added accordingly for the varying concentrations.

2.4. Characterization of GO/Zn(OH)x Composite

The morphology of the GO/Zn (OH)x nanocomposite was investigated using a Sigma VP Carl Zeiss scanning electron microscope (Carl Zeiss, White Plains, NY, USA). The samples were sputter coated with a thin layer of gold and palladium using Denton's Desk V deposition system.

Energy Dispersive Spectroscopy (EDS) (EDAX, Mahwah, NJ, USA) was used to analyze the elemental composition of the nanocomposite. Elemental mapping and EDS spectra analysis were used to observe C, O, and Zn in the samples.

The crystal structure of the synthesized GO and Zn (OH)x nanoparticles was examined by XRD. A Bruker D2 powder X-ray diffractometer was used with a Co source (Kα 1.789 Å). The XRD was filtered using an iron film. The data were collected in 2θ from 5 to 75° with a count time of 5 sec and a step of 0.05° in 2θ.

The antibacterial activity of the GO/Zn (OH)x nanocomposite was evaluated against Gram-positive bacteria *B. megaterium* and Gram-negative bacteria *Escherichia coli.* The Kirby Bauer disk diffusion method was used as standard. A 100 µL suspension of bacteria was injected onto an agar plate. The bacterial solution of 100 microliters transferred to each petri dish contained approximately 2×10^6 viable cells, where a sufficient amount was added to produce a lawn on the surface of the Milton Hilton agar. This amount gave visible clear zones of inhibition. The number of cells applied to the plates was confirmed by the ten-fold dilution method. The bacteria were spread out evenly on the plate using a sterile L-shaped glass rod; the NPs were placed on the surface of the plates using sterile forceps. Finally, the agar plates with NPs were left in an incubator at 37 °C for 48 h.

3. Results and Discussion

3.1. Morphology

Figure 1A shows the morphology of the GO, which appears to have some platelets present in the image and some large ball-like cluster structures. It is also observed in Figure 1A that some very thin sheets are present on the top left of the image, showing the typical crinkled sheets of graphene oxide. The modified Hummer's synthesis method has shown similar results [19,54]. Shahriary et al. reported folded ultra-thin films with crinkled edges [55]. Figure 1B shows the decoration of 25% Zn (OH)x on the GO sheets. The appearance of the 25% ZnO-GO composite shows a structure that is very similar to that of the GO, with the presence of large ball-like clusters, and some small plate-like structures are also present. The SEM image of the 50% Zn (OH)x GO composite sample (Figure 1C) shows a broken sheet-like structure. There are some bright spots present on the sample, which are visible NPs on the surface of the GO sheets, which may be due to the readiness of preferable sites for the growth of Zn(OH)x [47]. Alternatively, the precipitation of the Zn $(OH)_2$ on the surface may be large particles/more crystalline and may be clustered. The 75% Zn (OH)x-GO composite material (Figure 1D) shows a structure similar to that of the 50% Zn (OH)x-GO composite/broken sheet structure. In addition, the edges of the broken sheets in the layers are visible on the surface, as are the small clusters of the Zn (which are the bright spots).

In fact, different samples are shown in Figure 1. The SEM image of the GO without Zn (OH)x is shown in Figure 1A, while the SEM images of GO coated with 25%, 50%, and 75% of Zn(OH)x are shown in Figures 1B, 1C and 1D, respectively. One would expect that the morphology of the GO will change as it reacts with Zn and OH ions. However, in all the samples, one can see some plate-like structures indicating the existence of graphene oxide. Figure 1A shows the graphene oxides extracted from the solution. In fact, the extracted graphene oxide from the solution would then be reacted with Zn and OH, where we would probably lose the smaller particles, and some digestion of the GO would happen to change the appearance somewhat. The possible digestion and loss of the smaller particles of GO would be to larger extents as the Zn and OH concentration was increased or the amount of Zn and OH increased. Thus, one would expect more large visible structures after the reaction of GO with higher concentrations of Zn and OH.

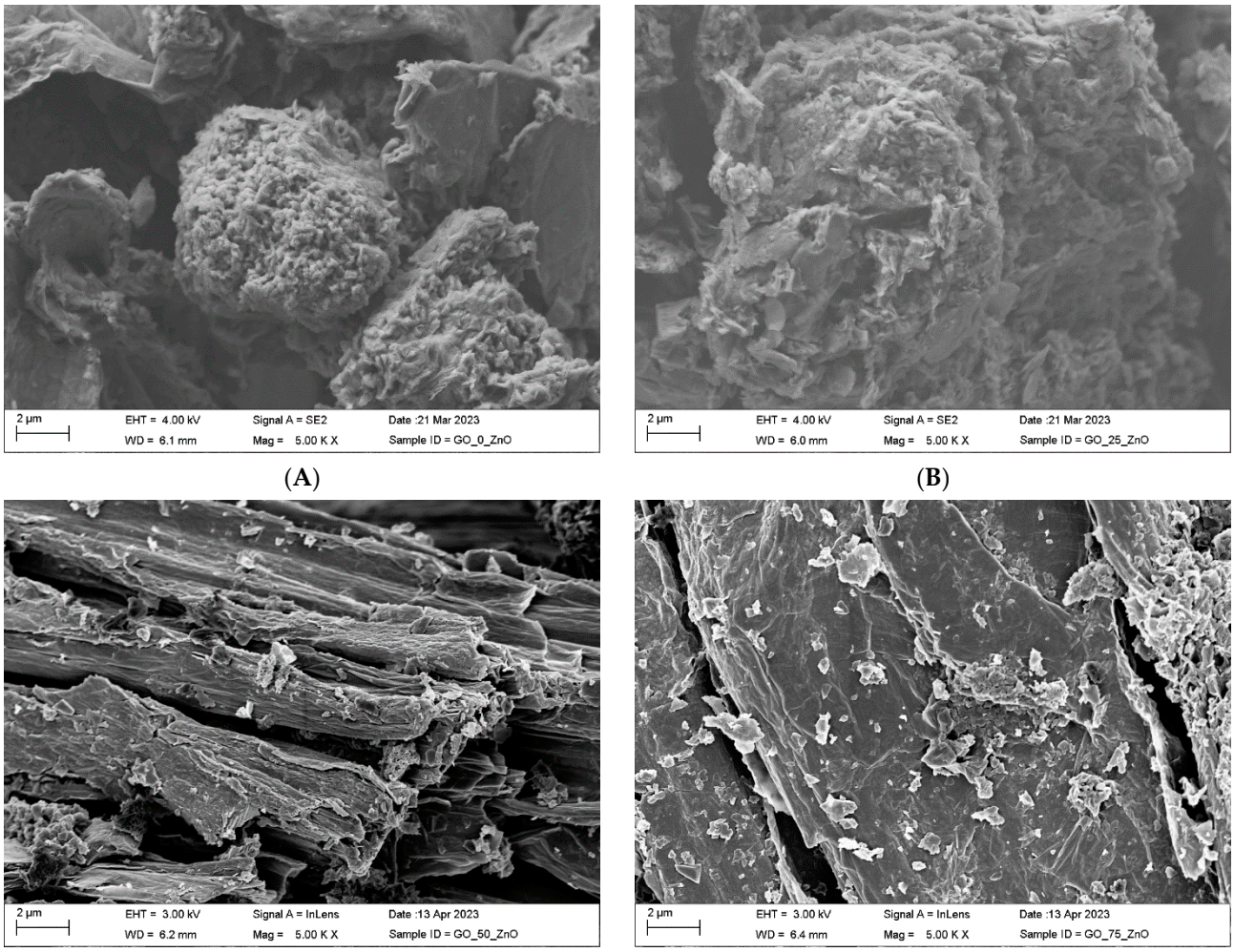

Figure 1. SEM images of GO/Zn (OH)x composite: (**A**) Non-coated GO. (**B**) GO with 25 wt.% Zn (OH)x. (**C**) GO with 50 wt.% Zn (OH)x and (**D**) GO with 75 wt.% Zn (OH)x coating.

3.2. Elemental Mapping

The elemental mapping and EDS analysis were performed on the GO/Zn (OH)x nanocomposite to investigate the elemental composition/homogeneity of the samples. Figures 2–5 show the EDS mappings of the non-coated GO and GO/Zn (OH)x composite materials. As can be seen in Figure 2, the C and the oxygen are homogeneously mixed throughout the samples, indicating a good oxidation of the graphite to form the GO. The EDS mappings of the 25% GO/Zn (OH)x composite (Figure 3) show a homogenous distribution of the C, O, and Zn throughout the sample. The EDS results of the 50% and 75% Zn (OH)x composites (Figure 4) again show a homogenous distribution of the C, O, and Zn in both samples. The homogenous mixture of the C, O, and Zn throughout all the composite samples indicates the presence of either a coated sample or a composite material. The results of the EDS analysis are shown in Table 1. The 25% Zn (OH)x composite shows that 14% of the sample was Zn. The 50% Zn (OH)x composite showed that the sample has a 37 wt.% of Zn present, while the 75% Zn (OH)x sample showed a 31 wt.% of Zn. The observed leveling-off from the Zn concentration in the 50 and 75% samples may be due to the surface site available for Zn binding on the GO.

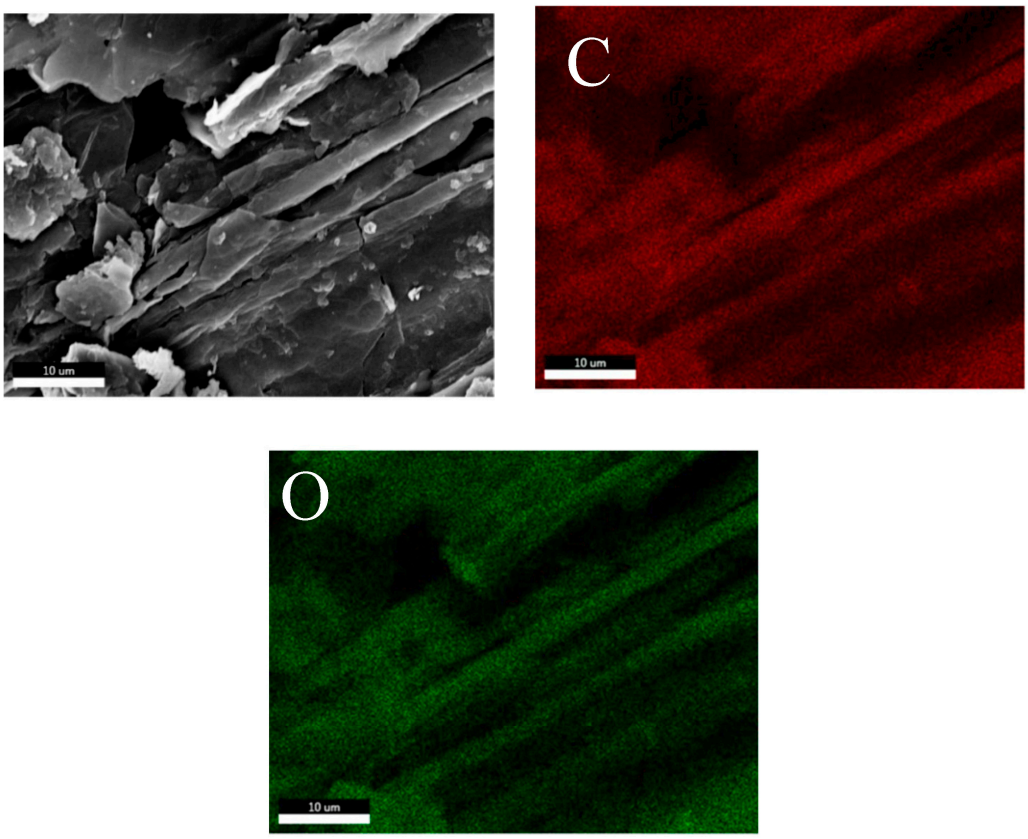

Figure 2. Elemental composition of non-coated GO.

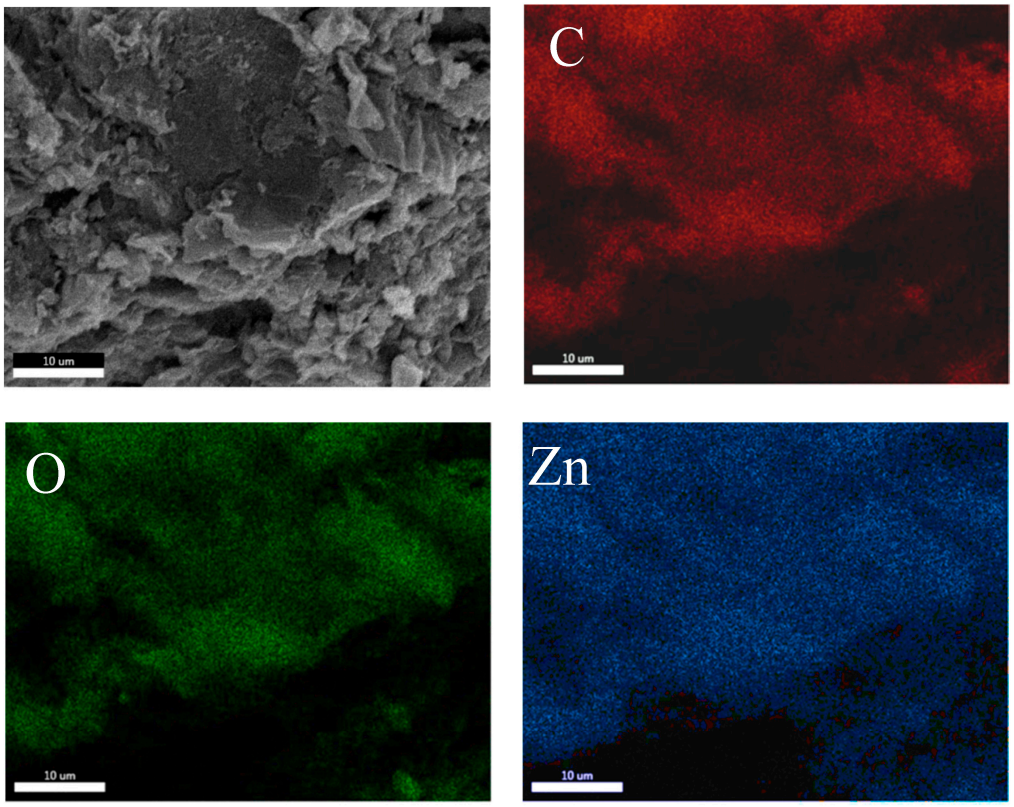

Figure 3. Elemental composition of GO with 25% Zn (OH)x coating.

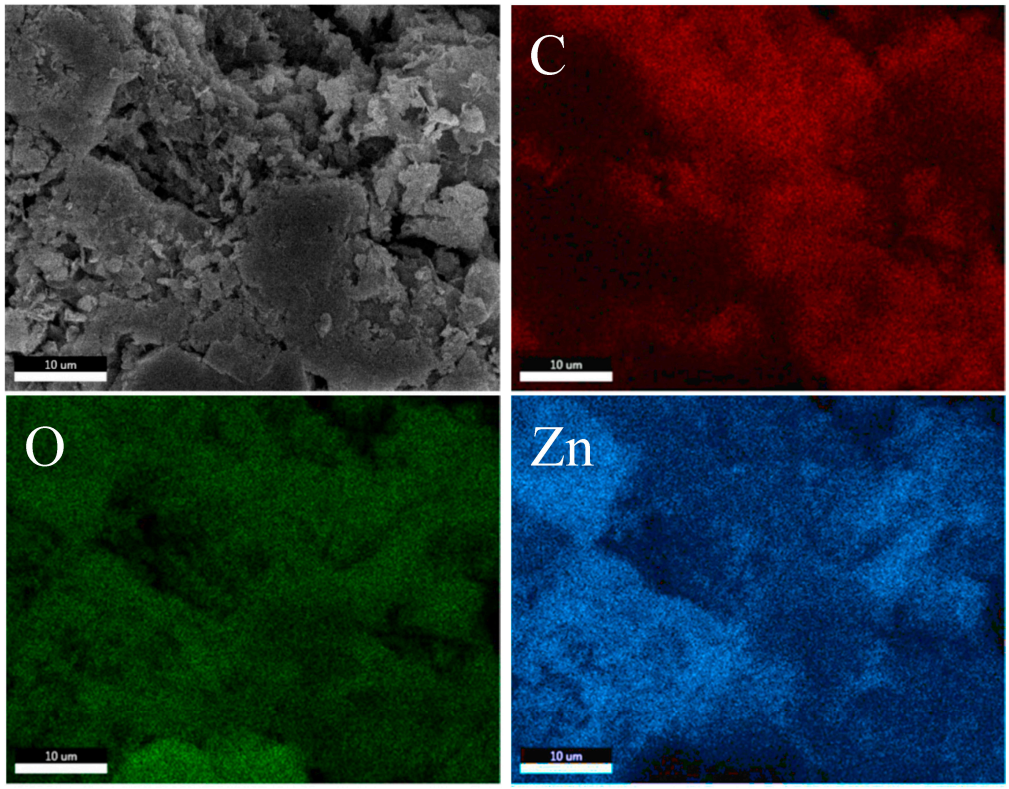

Figure 4. Elemental composition of GO with 50% Zn (OH)x coating.

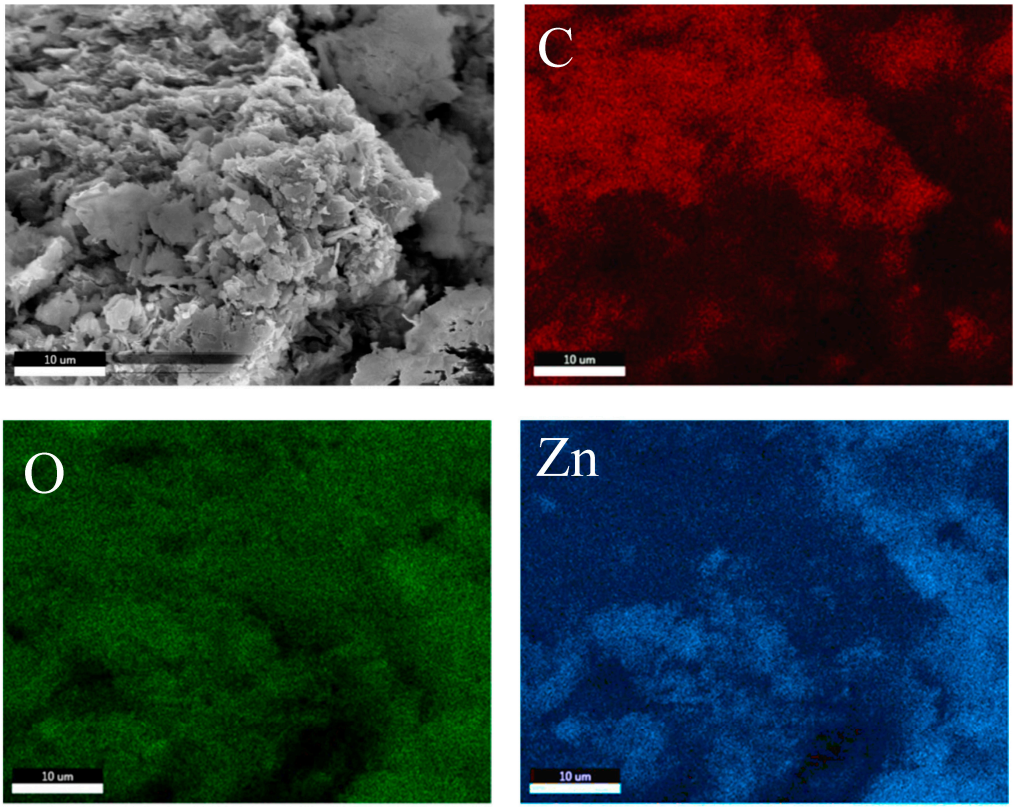

Figure 5. Elemental composition of GO with 75% Zn (OH)x coating.

Table 1. EDS results of non-coated GO and GO coated with 25, 50, and 75 wt.% of Zn(OH)x.

Sample	Element (Shell)	Weight (%)	Atomic (%)	Net Int.	Error (%)	Kratio	Z	A	F
GO	C(K)	58.24	65.01	637.70	3.86	0.48	1.02	0.81	1.00
	O (K)	41.76	34.99	351.20	7.88	0.17	0.97	0.43	1.00
GO-25% Zn (OH)x	C (K)	58.88	71.86	593.00	5.73	0.39	1.06	0.62	1.00
	O (K)	27.34	25.05	253.90	8.39	0.11	1.00	0.40	1.00
	Zn (L)	13.77	3.09	121.60	3.24	0.09	0.72	0.95	1.00
GO-50% Zn (OH)x	C (K)	33.93	54.48	410.00	7.96	0.16	1.15	0.40	1.00
	O (K)	28.59	34.46	595.20	7.28	0.15	1.09	0.48	1.00
	Zn (L)	37.47	11.06	607.50	2.78	0.27	0.78	0.93	1.00
GO-75% Zn (OH)x	C (K)	40.89	60.69	654.60	7.47	0.21	1.13	0.45	1.00
	O (K)	27.56	30.71	650.40	7.48	0.13	1.07	0.45	1.00
	Zn (L)	31.54	8.60	614.40	2.69	0.23	0.77	0.94	1.00

3.3. X-ray Diffraction

Figure 6 shows the XRD pattern of the synthesized graphene oxide and the GO/$Zn(OH)_x$ nanocomposite materials (A). The diffraction pattern of the synthesized graphene oxide shows a typical diffraction pattern of GO. The expansion of the graphite lattice along the c-axis causes the graphite 002 peak to shift and become the GO 001 peak located at 11.68 in 2θ [56,57]. This is a consequence of the oxidation of the surface of the layers in the graphite, which caused expansion of the c-axis in the crystal (the 002 plane in graphite); as the expansion is large, the 002 peak moves lower in diffraction angle, which indicates an increase in the interplanar graphite spacing and for some reason, it is named the 001 peak [57–59].

Figure 6B shows the Le Bail fitting of the graphene oxide sample, which shows a good agreement between the literature and the fitting results, as indicated by the low χ^2 value in Table 2 of 1.13. Also, there is evidence of the presence of some residual graphite in the sample after synthesis, as is evidenced by the small peak at 31.26 in 2θ [53]. It can be seen in Figure 6B that the synthesized GO/Zn $(OH)_x$ composite materials exhibit a diffraction pattern consisting of numerous peaks. The composition of the GO/Zn $(OH)_x$ composite samples was determined to be a combination of three components, which were graphene oxide, ϵ-Zn $(OH)_2$, and $Zn_5(OH)_{10}$ $2H_2O$. In addition, it should be noted that the GO peak has shifted to a slightly higher diffraction angle, which indicates a slight compression in the length of the C-axis. The compression of the C-axis of the crystal is also evidenced by the small shift in the diffraction pattern for the GO 001 peak from 11.68 to 12.78 ° in 2θ. This change in the diffraction angle indicates a 0.4 Å decrease in the interplanar spacing of the graphene oxide. This compression of the structure may be due to the removal of smaller pieces of graphene oxide after the reaction with the Zn^{2+} and the OH^- ions in the solution. Alternatively, it may be caused by the fact that some of the groups changed after the reaction, causing the planes to come closer together.

Table 2. Results of Le Bail fitting of GO, Zn-75-GO, and graphite.

Sample	Phase	Space Group	a (Å)	b (Å)	c (Å)	α (°)	β (°)	γ (°)	χ^2
Zn-75-G.O.	$Zn_5(OH)_{10}2H_2O$	C2/c	15.32 (3)	6.10 (1)0	10.96 (2)	90.00	99.10	90.00	
	ϵ-Zn $(OH)_2$	$P2_12_12_1$	4.18 (5)	5.04 (8)	8.52 (4)	90.00	90.00	90.00	2.03
	G.O.	$P6_3mc$	2.48 (4)	2.48 (4)	16.62	90.00	90.00	120.00	
Graphene Oxide	G.O.	$P6_3mc$				90.00	90.00	120.00	1.13
	Graphite	$P6_3mc$	2.45 (3)	2.45 (3)	6.64 (9)	90.00	90.00	120.00	

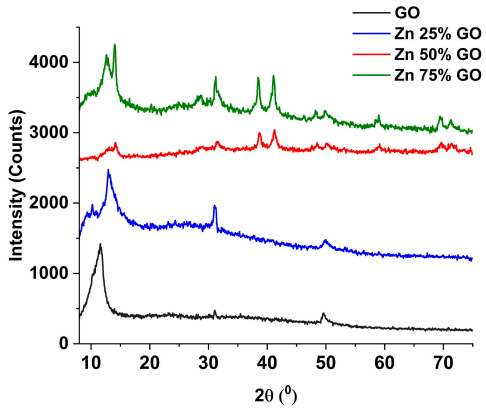

(**A**)

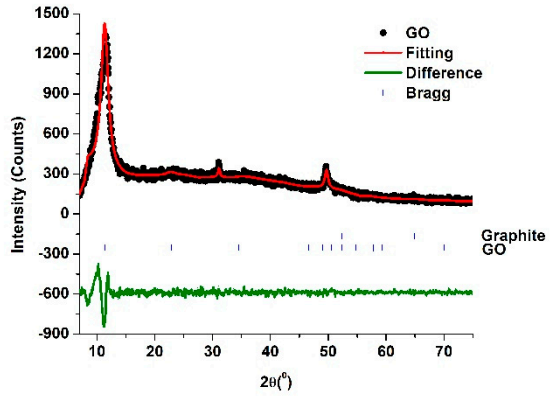

(**B**)

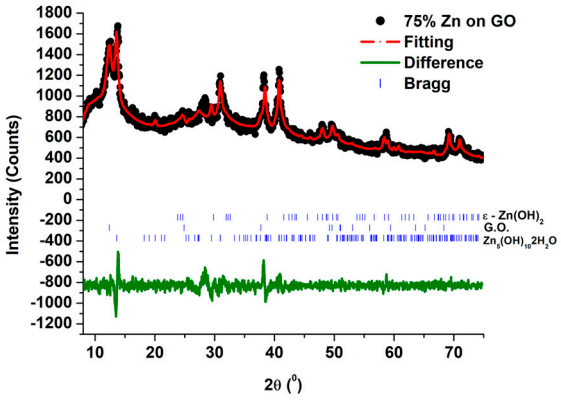

(**C**)

Figure 6. (**A**) XRD diffraction of GO and and GO/Zn $(OH)_x$ composites; (**B**) Le Bail fitting of the diffraction pattern collected for the GO sample; (**C**) Le Bail fitting of the diffraction pattern for the GO/Zn $(OH)_x$ 75 wt.% sample.

The composition was determined using the Le Bail fitting procedure in the Fullprof software (Version 5.10) and crystallographic data from the literature [60]. The Le Bail fitting of the GO/Zn $(OH)_{x-75}$ is shown in Figure 6C and the results of the fitting are presented in Table 2. The Le Bail fitting had a χ^2 of 2.03, which indicates a good agreement between the literature values and the experimental data [26,59,61,62]. The lattice values are also within a reasonable error of the literature crystal structures.

3.4. XPS Results

Figure 7A–D show the C 1s XPS spectrum of the GO/Zn $(OH)_x$ samples with different Zn $(OH)_x$ concentrations of 0, 25, 50, and 75 wt%, respectively. The C1S XPS results showed a peak centered around 285.7 eV, which was deconvolved into three separate peaks located at 284.2, 285.7, and 287.7. These peaks represent the C-C/C=C, the C-O, and the C=O coordination environments [63,64]. No large changes were observed in the binding environment of the graphene oxide, indicating that the Zn is not directly attached to the carbon in the graphene oxide sheets.

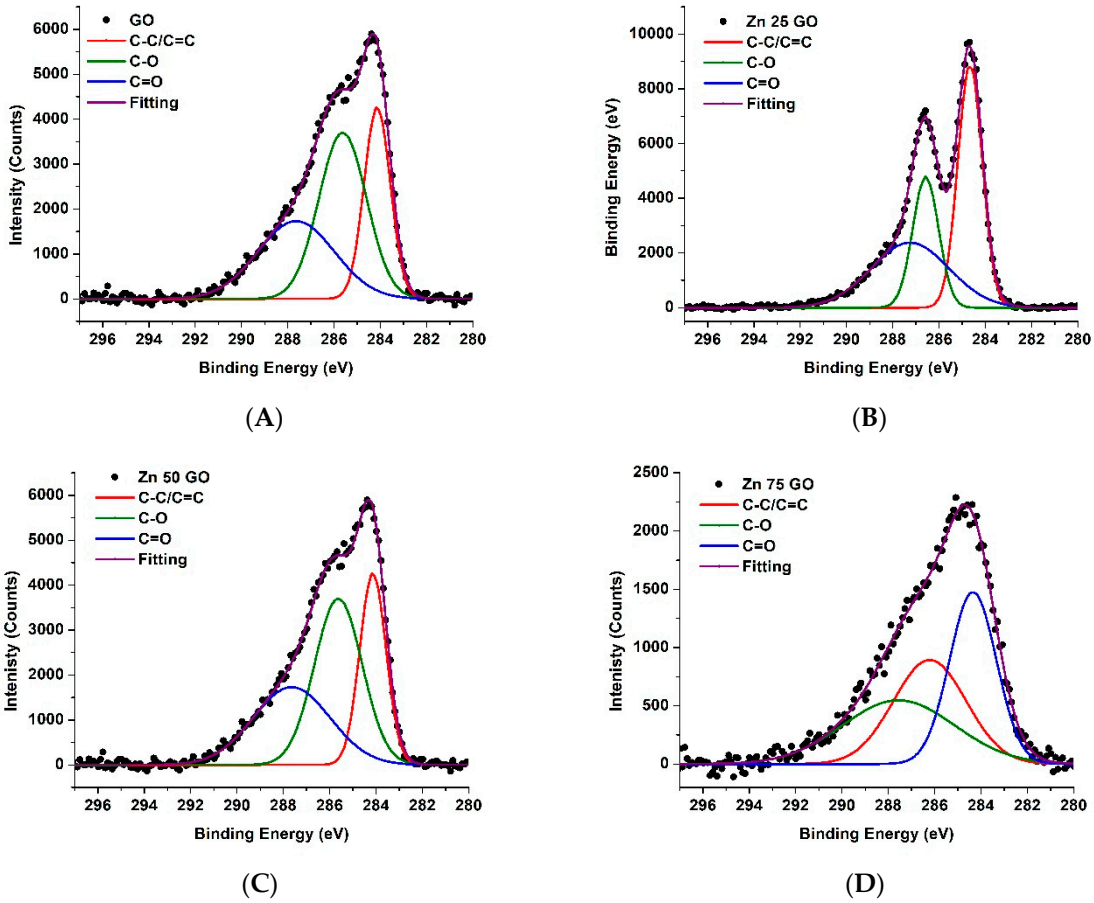

Figure 7. C 1s XPS spectrum of the GO/Zn $(OH)_x$ samples with different Zn $(OH)_x$ concentrations of: (**A**) (0 wt. %), (**B**) (25 wt.%), (**C**) (50 wt.%), and (**D**) (75 wt.%).

Figure 8A–D show the O1S XPS spectrum of the GO/Zn $(OH)_x$ samples with Zn $(OH)_x$ concentrations of 0, 25, 50, and 75 wt.%, respectively. The O1 spectra showed a peak centered around 523 eV, which was deconvolved into three peaks located at 531.3, 532.4, and 533.2 eV for the GO sample. These peaks were consistent with the binding environments for the C-O, OH, and C=O, respectively. The XPS results in Figure 8A are consistent with those reported in the literature on graphene oxide. Interestingly, when the main peak of the O1 spectra was deconvolved for each of the GO/Zn $(OH)_x$ samples, a slight shift in the peak was observed with changing Zn $(OH)_x$ concentration. For the GO/Zn $(OH)_x$ sample with 25 wt.% concentration, the O1S spectrum was deconvolved into three peaks located at 531.5, 532.5, and 533.2 eV, which were consistent with O-Zn/O-H, C-OH, and C=O binding environments [63,64]. The O1S peak of the GO/Zn $(OH)_x$ samples with 50 and 75 wt.% of $Zn(OH)_X$ (Figure 8C) was deconvolved into two individual peaks located at 531.9 and 534.1, which were consistent with Zn-OH and C-O/C=O binding environments [65,66].

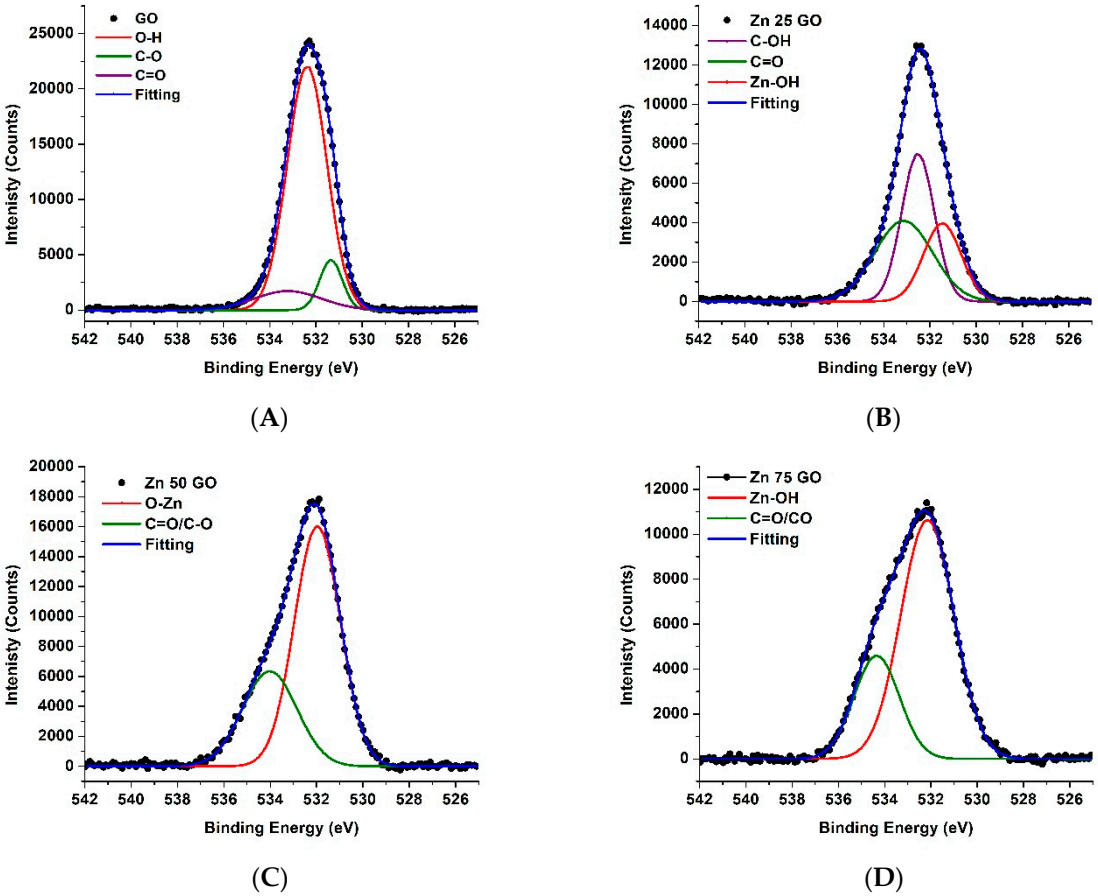

Figure 8. O1S XPS spectrum of the GO/Zn (OH)x samples with different Zn (OH)x concentrations: (**A**) (0 wt. %), (**B**) (25 wt.%), (**C**) (50 wt.%), and (**D**) (75 wt.%).

Figure 9A–C show the Zn $2P_{3/2}$ and Zn $2P_{1/2}$ XPS spectra for the GO/Zn (OH)x samples with different Zn $(OH)_X$ concentrations of 0, 25, 50, and 75 wt%, respectively. The Zn 2P showed two peaks centered around 1022.4 and 1045.7 eV, representing the Zn $2P_{3/2}$ and Zn2 $P_{1/2}$ binding energies, respectively. The Zn2 $P_{3/2}$ peak was deconvolved into two peaks, which were centered around 1022.2 and 1024.5 eV. The two $Zn2P_{3/2}$ peaks indicated that the Zn is present as the Zn^{2+} and is bound to an oxygen ligand on graphene oxide [67,68]. It is well-known that the shifts in XPS peaks are common due to many factors, such as a metal binding to a specific site or complex formation or the formation of nanoparticles and size, and the latter is a well-known contributor to binding energy. Interestingly, the shifts away from the peak observed for the GO indicate that the oxygen functional groups are involved in the binding of the Zn2+ ions to the GO [69,70]. In fact, shifts in the O1s spectrum, up to 534 eV, have been observed in the literature for transition metals bound to graphene oxide as well as in the formation of Zn(hydroxy)oxide–GO composites [71].

The results reported by Kumar et al. showed that the binding of Zn onto biochar had a binding energy of 1024 eV in aged biochar, indicating that the binding occurs through an oxygen moiety [72]. The attachment of the Zn to the graphene oxide is through the oxygen on the surface, which was indicated in the appearance of the O-Zn bond observed in the O1S spectrum. The Zn $2P_{1/2}$ spectrum represents the same information as in the binding of the Zn-O on the graphene oxide surface (1047.5 eV) and the presence of the Zn-OH located at (1045.2 eV).

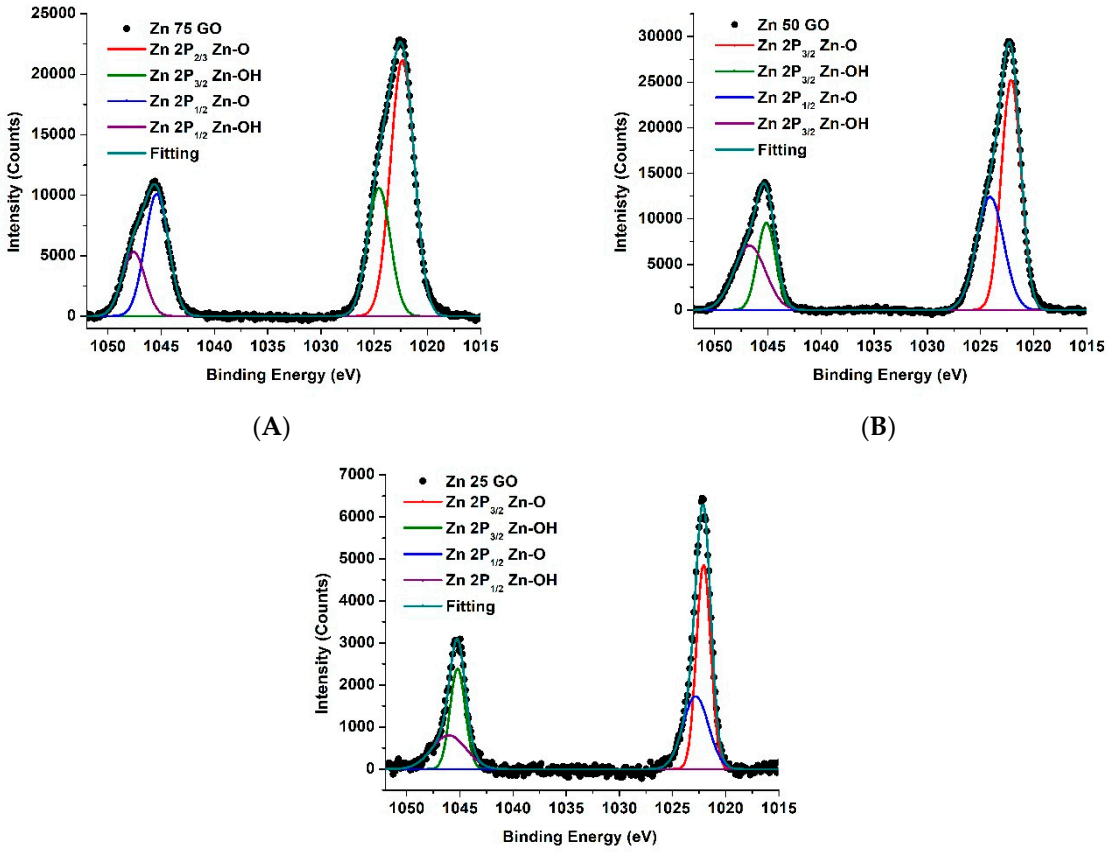

Figure 9. Zn $2P_{3/2}$ and $Zn2P_{1/2}$ XPS spectra for the GO/Zn (OH)x samples with different Zn (OH)x concentrations: of (**A**) (25 wt.%), (**B**) (50 wt.%), and (**C**) (75 wt.%).

3.5. Antibacterial Performance

To observe their effectiveness as antibacterial agents, GO/Zn $(OH)_x$ nanocomposite with various amounts of Zn $(OH)_x$ coatings was evaluated against both Gram-positive *B. megaterium* and Gram-negative *E. coli* bacteria. The disk diffusion method was used to observe the inhibition zone of the GO/Zn $(OH)_x$ nanocomposite with different concentrations of Zn(OH)x. In this method, the samples were placed on agar plates with the bacteria and incubated for 48 h at 37 °C. The size of the inhibition zone was measured using the ImageJ software (version 1.53t). The resulting inhibition zone growth can be observed in Figure 10A–D and Figure 11A–D, respectively.

The results in Figures 10 and 11 show clearly that the GO/Zn $(OH)_x$ composites inhibited the growth against both *E. coli* and *B. megaterium* bacteria. The inhibition zone growth capacity after 48 h of the GO/Zn $(OH)_x$ nanocomposite samples with 0, 25, 50, and 75 wt. % of Zn (OH)x against Gram-positive, *B. megaterium* bacteria (Figure 10) was 43.67, 47.07, 69.79, and 77.01%, respectively. The antibacterial activity results (Figure 11) of GO/Zn $(OH)_x$ nanocomposites against Gram-negative *E. coli* showed inhibition zone efficiency of 19.07, 33.44, 53, and 57.47% for 0, 25, 50, and 75 wt. % Zn $(OH)_x$ coating concentrations, respectively.

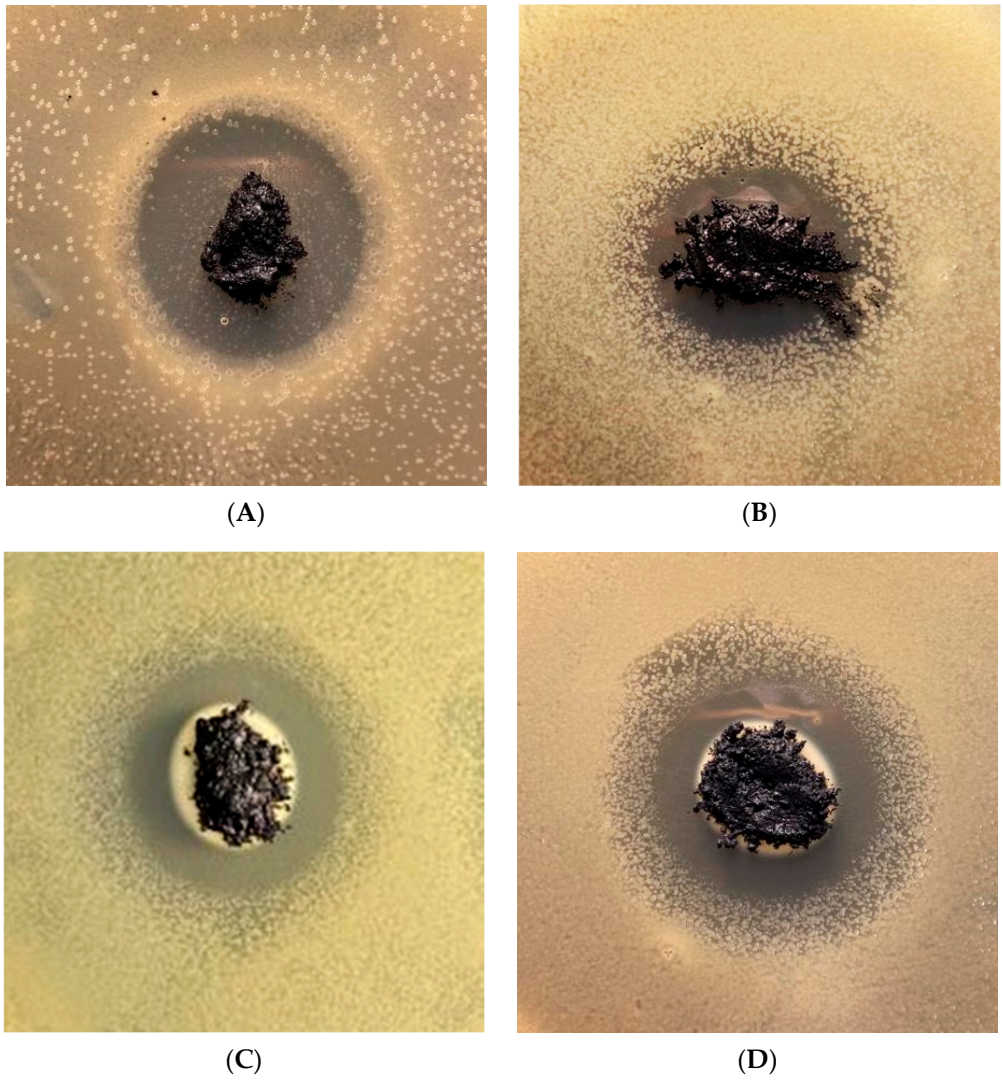

Figure 10. Inhibition zone against *B. megaterium* of GO/Zn (OH)x nanocomposites with different coating amounts of Zn $(OH)_x$: (**A**) 0%, (**B**) 25%, (**C**) 50%, and (**D**) 75 wt. %.

The antibacterial efficiency of GO has been reported previously to show good antibacterial activity against *E. coli* [17]. Our antibacterial activity results shown in Figures 10 and 11 are similar to those reported on Al/GO composite against Gram-negative strain *E. coli* [73] and Ag/CuO/GO nanocomposites against Gram-negative strain *E. coli* and Gram-positive *S. aureus* [74]. In fact, the results shown in Figures 11 and 12 confirm that the Zn $(OH)_x$ coating improved the antibacterial activity of GO against *B. megaterium* and *E. coli* bacteria. The relationship between the coating concentration of $Zn(OH)_x$ on GO and the growth of inhibition was positive. Also, the zone of inhibition was significantly larger in the Gram-positive bacteria for the GO/Zn $(OH)_x$ composite. This could be attributed to the fact that Zn $(OH)_x$ performs exceptionally well against Gram-positive bacteria [75–80]. Table 3 illustrates the inhibition zone diameter with the standard deviation of the GO/Zn (OH)x composite samples with different concentrations of Zn (OH)x NPs. Table 3 clearly shows the substantial positive progression from the initial zone of inhibition of the non-coated GO to GO with 75% Zn $(OH)_x$ coating. The initial zone of inhibition for the non-coated GO was 1.93 cm and increased to 4.82 cm against the Gram-positive *B. megaterium*. There was also an increase in the inhibition zone diameter for *E. coli* from 1.34 cm to 2.41 cm. The results shown in Figures 10–12 confirm that GO/Zn $(OH)_x$ composites have good and improved antibacterial properties compared to the pristine GO. In fact, the results reported in this study on the antibacterial properties of GO and GO/Zn(OH)x nanocomposites are

in agreement with those reported on different/similar systems [81,82]. The addition of zinc dehydrates to GO improved its antibacterial properties (Figure 12). These results are consistent with the fact that combining metal or metal oxides with Gr, rGO, or graphene can result in a synergetic effect of the composite by increasing the inhibition zone and the toxicity of the matrix (GO) and, therefore, preventing bacterial infection. The results reported in the literature on ZnO NPs [83] and GO/ZnO and RGO/ZnO nanocomposites [84] against *E. coli* have proven that increasing the amount of ZnO in the GO/ZnO composite resulted in increased inhibition zone, which is similar to our finding in the present manuscript. The improved antibacterial properties of ZnO/GO nanocomposites were attributed to the combined activation of mechanisms of Zn ions from ZnO and the physical interaction between the GO sharp edge and *E.coli* [84]. In fact, the addition of metallic ions (+) to GO, rGO and/or graphene will definitely improve the antibacterial properties of these materials due to the synergetic effect of metallic ions when combined with GO or rGO [85,86].

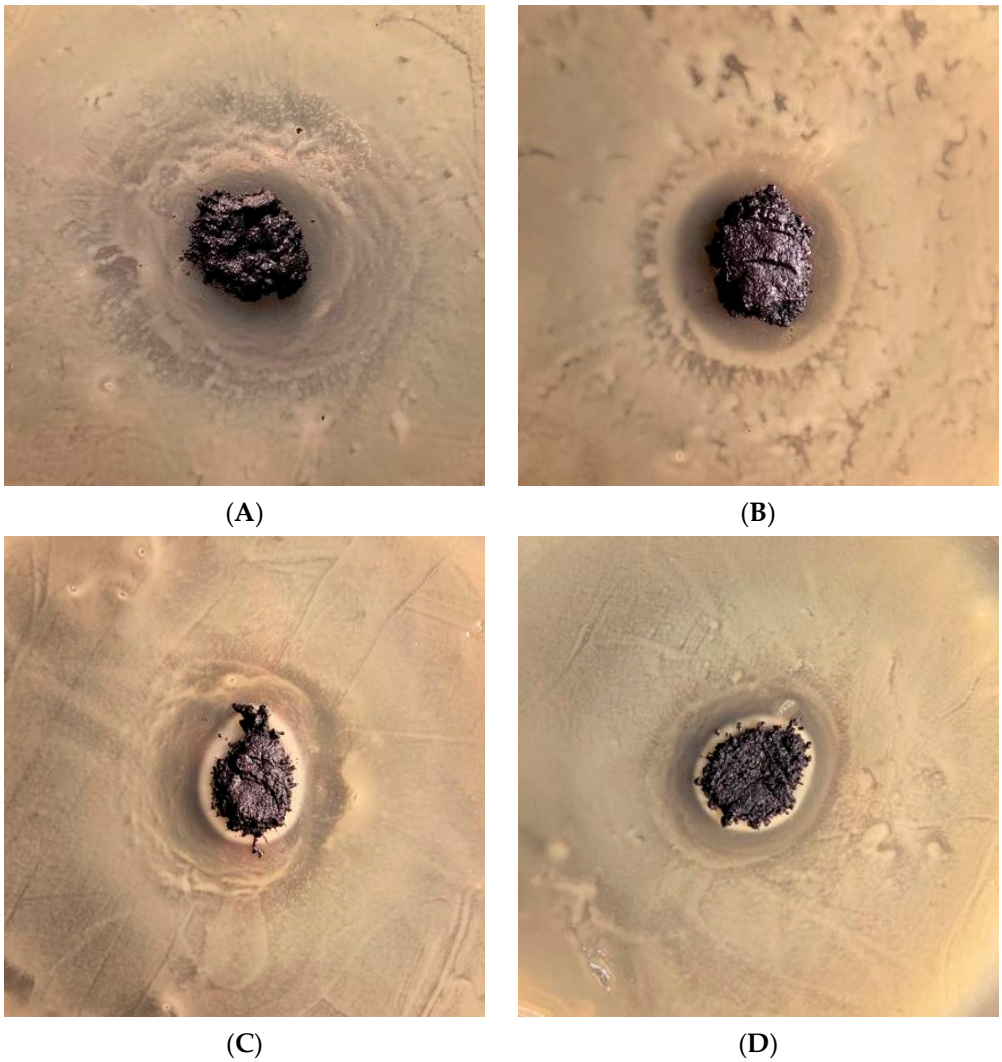

(**A**) (**B**)

(**C**) (**D**)

Figure 11. Inhibition zone against *E. coli* bacteria of GO/Zn (OH)x nanocomposites with different coating amounts of Zn (OH)x: (**A**) 0%, (**B**) 25%, (**C**) 50%, and (**D**) 75 wt. %.

It is important to note here that the GO/Zn $(OH)_x$ composites synthesized in this work can eventually be applied to a bacterially contaminated environment. In fact, the GO and GO/Zn (OH)x nanocomposite can be applied to a bacterially contaminated environment as an antibacterial soap or oil since ZnO and Zn (OH)x cannot dissolve in water. Zinc oxide is not soluble in water; thus, it requires oil or other such carrier agents to function effectively. The nanocomposite can also be used as wipes or in the form of particles dispersed in

gel. However, we are still in the early stages of applying the material as a commercial antibacterial agent. This requires more work and research to achieve this goal.

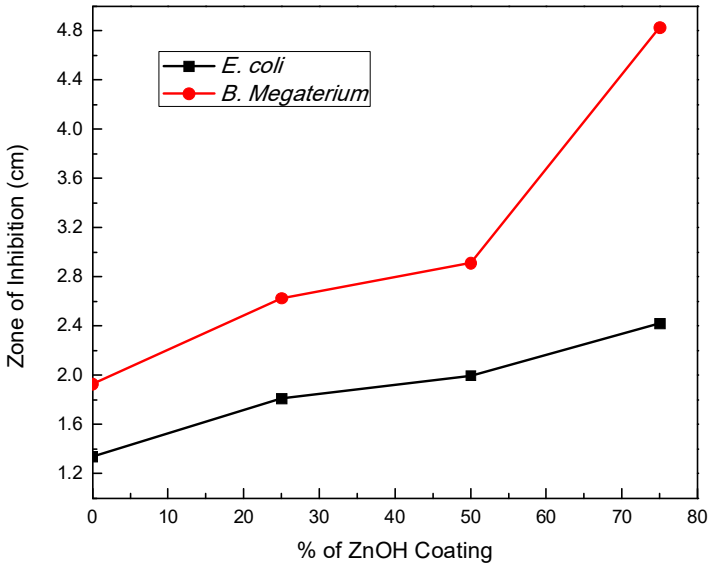

Figure 12. Relationship between Zn (OH)x coating concentration on GO and their inhibition zone diameters.

Table 3. Zone of Inhibition of various GO/Zn $(OH)_x$ composite NPs.

	B. megaterium		*E. coli*	
% Coating	**Zone of Inhibition**	**Standard Deviation**	**Zone of Inhibition**	**Standard Deviation**
0	1.9277	0.118541	1.3372	0.066645
25	2.6266	0.089994	1.8097	0.048761
50	2.9097	0.069652	1.9962	0.057996
75	4.8273	0.127387	2.4175	0.08373

4. Conclusions

Graphene oxide was successfully synthesized using the modified Hummers' method. The GO was then coated with different concentrations of Zn (OH)x to study the effect of Zn (OH)x coating on the antibacterial activity of GO against Gram-positive *B. megaterium* and Gram-negative *E. coli* bacteria. The GO/Zn $(OH)_x$ nanocomposites were characterized using different methods. The GO/Zn $(OH)_x$ composites exhibited a hybrid stacked sheet structure with some agglomerations of Zn $(OH)_x$ on the surface. The XRD and XPS analysis effectively confirmed the presence of Zn $(OH)_x$ in the GO/Zn $(OH)_x$ nanocomposites. The antibacterial results showed inhibition on both Gram-negative *E. coli* and Gram-positive *B. megaterium*. However, the GO/Zn $(OH)_x$ nanocomposite had larger inhibition zones against the Gram-positive *B. megaterium*. There was also a significant increase in the inhibition zone with increasing the amount of Zn $(OH)_x$ coating against the Gram-positive bacteria. The same positive trend was observed against the Gram-negative bacteria. Although there was an increase in the inhibition zone, it was not as significant as the increase for the Gram-positive bacteria case. Zinc hydroxide has been observed to perform better against Gram-positive bacteria, and the results further confirmed that behavior.

Author Contributions: Conceptualization, M.A. and J.G.P.; Methodology, M.A. and J.A.S.; Formal Analysis, J.A.S., J.G.P., L.M. and M.A.; Investigation, J.A.S., L.M. and M.A.; Resources, M.A., L.M. and J.G.P.; Data Curation, M.A. and J.G.P.; Writing—Original Draft Preparation, J.A.S.; Writing—Review & Editing, M.A. and J.G.P.; Supervision, J.G.P. and M.A.; Project Administration, M.A.; Funding Acquisition, J.G.P. and M.A. All authors have read and agreed to the published version of the manuscript.

Funding: M.A. acknowledges funding from NSF PREM (DMR-2122178), Partnership for Fostering Innovation by Bridging Excellence in Research and Student Success. M. Alcoutlabi also acknowledges the funding from the Lloyd M. Bentsen, Jr. Endowed Chair in Engineering endowment at UTRGV. J.G. Parsons acknowledge and are grateful for the support provided by the UTRGV Chemistry Departmental Welch Foundation Grant (Grant No. BX-0048).

Institutional Review Board Statement: This study did not require ethical approval.

Informed Consent Statement: This study did not involve humans.

Data Availability Statement: All the relevant data that support the findings of this study are available from the corresponding author on reasonable request.

Acknowledgments: This work was supported by the Lloyd M. Bentsen, Jr. Endowed Chair in Engineering endowment at UTRGV. This work was also supported by the National Science Foundation (NSF) PREM award under grant no. DMR-2122178: UTRGV-UMN Partnership for Fostering Innovation by Bridging Excellence in Research and Student Success. J.G. Parsons acknowledges and is grateful for the support provided by funding from the UTRGV Chemistry Departmental Welch Foundation Grant (Grant No. BX-0048).

Conflicts of Interest: The authors declare no conflict of interest.

References

1. Rahman, S.; Sadaf, S.; Hoque, M.E.; Mishra, A.; Mubarak, N.M.; Malafaia, G.; Singh, J. Unleashing the promise of emerging nanomaterials as a sustainable platform to mitigate antimicrobial resistance. *RSC Adv.* **2024**, *14*, 13862–13899. [CrossRef] [PubMed]
2. Moradi, F.; Ghaedi, A.; Fooladfar, Z.; Bazrgar, A. Recent advance on nanoparticles or nanomaterials with anti-multidrug resistant bacteria and anti-bacterial biofilm properties: A systematic review. *Heliyon* **2023**, *9*, e22105. [CrossRef] [PubMed]
3. Makabenta, J.M.V.; Nabawy, A.; Li, C.H.; Schmidt-Malan, S.; Patel, R.; Rotello, V.M. Nanomaterial-based therapeutics for antibiotic-resistant bacterial infections. *Nat. Rev. Microbiol.* **2021**, *19*, 23–36. [CrossRef]
4. Kumar, P.; Huo, P.P.; Zhang, R.Z.; Liu, B. Antibacterial Properties of Graphene-Based Nanomaterials. *Nanomaterials* **2019**, *9*, 737. [CrossRef] [PubMed]
5. Frei, A.; Verderosa, A.D.; Elliott, A.G.; Zuegg, J.; Blaskovich, M.A.T. Metals to combat antimicrobial resistance. *Nat. Rev. Chem.* **2023**, *7*, 202–224. [CrossRef] [PubMed]
6. Badoni, A.; Prakash, J. Noble metal nanoparticles and graphene oxide based hybrid nanostructures for antibacterial applications: Recent advances, synergistic antibacterial activities, and mechanistic approaches. *Micro Nano Eng.* **2024**, *22*, 100239. [CrossRef]
7. Ji, H.; Sun, H.; Qu, X. Antibacterial applications of graphene-based nanomaterials: Recent achievements and challenges. *Adv. Drug Deliv. Rev.* **2016**, *105*, 176–189. [CrossRef] [PubMed]
8. Lee, J.; Kim, J.; Kim, S.; Min, D.-H. Biosensors based on graphene oxide and its biomedical application. *Adv. Drug Deliv. Rev.* **2016**, *105*, 275–287. [CrossRef]
9. Choi, S.; Kim, C.; Suh, J.M.; Jang, H.W. Reduced graphene oxide-based materials for electrochemical energy conversion reactions. *Carbon Energy* **2019**, *1*, 85–108. [CrossRef]
10. Thakur, K.; Kandasubramanian, B. Graphene and Graphene Oxide-Based Composites for Removal of Organic Pollutants: A Review. *J. Chem. Eng. Data* **2019**, *64*, 833–867. [CrossRef]
11. Chavez, R.O.; Lodge, T.P.; Huitron, J.; Chipara, M.; Alcoutlabi, M. Centrifugally spun carbon fibers prepared from aqueous poly(vinylpyrrolidone) solutions as binder-free anodes in lithium-ion batteries. *J. Appl. Polym. Sci.* **2021**, *138*, 50396. [CrossRef]
12. Flores, D.; Villarreal, J.; Lopez, J.; Alcoutlabi, M. Production of carbon fibers through Forcespinning® for use as anode materials in sodium ion batteries. *Mater. Sci. Eng. B Adv.* **2018**, *236*, 70–75. [CrossRef]
13. Worku, A.K.; Ayele, D.W. Recent advances of graphene-based materials for emerging technologies. *Results Chem.* **2023**, *5*, 100971. [CrossRef]
14. Xu, M.S.; Liang, T.; Shi, M.M.; Chen, H.Z. Graphene-Like Two-Dimensional Materials. *Chem. Rev.* **2013**, *113*, 3766–3798. [CrossRef]
15. Ji, L.W.; Meduri, P.; Agubra, V.; Xiao, X.C.; Alcoutlabi, M. Graphene-Based Nanocomposites for Energy Storage. *Adv. Energy Mater.* **2016**, *6*, 1502159. [CrossRef]
16. Smith, A.T.; LaChance, A.M.; Zeng, S.S.; Liu, B.; Sun, L.Y. Synthesis, properties, and applications of graphene oxide/reduced graphene oxide and their nanocomposites. *Nano Mater. Sci.* **2019**, *1*, 31–47. [CrossRef]

17. Liu, S.B.; Zeng, T.H.; Hofmann, M.; Burcombe, E.; Wei, J.; Jiang, R.R.; Kong, J.; Chen, Y. Antibacterial Activity of Graphite, Graphite Oxide, Graphene Oxide, and Reduced Graphene Oxide: Membrane and Oxidative Stress. *ACS Nano* **2011**, *5*, 6971–6980. [CrossRef] [PubMed]
18. Yaragalla, S.; Bhavitha, K.B.; Athanassiou, A. A Review on Graphene Based Materials and Their Antimicrobial Properties. *Coatings* **2021**, *11*, 1197. [CrossRef]
19. Rhazouani, A.; Gamrani, H.; El Achaby, M.; Aziz, K.; Gebrati, L.; Uddin, M.S.; Aziz, F. Synthesis and toxicity of graphene oxide nanoparticles: A literature review of in vitro and in vivo studies. *BioMed Res. Int.* **2021**, *2021*, 5518999. [CrossRef]
20. Zheng, H.; Ma, R.; Gao, M.; Tian, X.; Li, Y.-Q.; Zeng, L.; Li, R. Antibacterial applications of graphene oxides: Structure-activity relationships, molecular initiating events and biosafety. *Sci. Bull.* **2018**, *63*, 133–142. [CrossRef]
21. Pulingam, T.; Thong, K.L.; Ali, M.E.; Appaturi, J.N.; Dinshaw, I.J.; Ong, Z.Y.; Leo, B.F. Graphene oxide exhibits differential mechanistic action towards Gram-positive and Gram-negative bacteria. *Colloids Surf. B Biointerfaces* **2019**, *181*, 6–15. [CrossRef] [PubMed]
22. Gurunathan, S.; Han, J.W.; Dayem, A.A.; Eppakayala, V.; Kim, J.-H. Oxidative stress-mediated antibacterial activity of graphene oxide and reduced graphene oxide in Pseudomonas aeruginosa. *Int. J. Nanomed.* **2012**, *7*, 5901–5914. [CrossRef] [PubMed]
23. Liao, K.-H.; Lin, Y.-S.; Macosko, C.W.; Haynes, C.L. Cytotoxicity of graphene oxide and graphene in human erythrocytes and skin fibroblasts. *ACS Appl. Mater. Interfaces* **2011**, *3*, 2607–2615. [CrossRef]
24. Li, M.N.; Chen, Z.F.; Yang, L.X.; Li, J.Y.; Xu, J.; Chen, C.; Wu, Q.; Yang, M.M.; Liu, T.L. Antibacterial Activity and Mechanism of GO/CuO/ZnO Coating on Ultrafine Glass Fiber. *Nanomaterials* **2022**, *12*, 1857. [CrossRef]
25. Mohammed, H.; Kumar, A.; Bekyarova, E.; Al-Hadeethi, Y.; Zhang, X.X.; Chen, M.G.; Ansari, M.S.; Cochis, A.; Rimondini, L. Antimicrobial Mechanisms and Effectiveness of Graphene and Graphene-Functionalized Biomaterials. A Scope Review. *Front. Bioeng. Biotech.* **2020**, *8*, 465. [CrossRef]
26. Liu, J.J.; Hull, S.; Ahmed, I.; Skinner, S.J. Application of combined neutron diffraction and impedance spectroscopy for structure and conductivity studies of LaMoO. *Nucl. Instrum. Meth. B* **2011**, *269*, 539–543. [CrossRef]
27. Gold, K.; Slay, B.; Knackstedt, M.; Gaharwar, A.K. Antimicrobial Activity of Metal and Metal-Oxide Based Nanoparticles. *Adv. Ther.* **2018**, *1*, 1700033. [CrossRef]
28. Li, Y.; Zhang, W.; Niu, J.; Chen, Y. Mechanism of Photogenerated Reactive Oxygen Species and Correlation with the Antibacterial Properties of Engineered Metal-Oxide Nanoparticles. *ACS Nano* **2012**, *6*, 5164–5173. [CrossRef]
29. Nanda, S.S.; Yi, D.K.; Kim, K. Study of antibacterial mechanism of graphene oxide using Raman spectroscopy. *Sci. Rep.* **2016**, *6*, 28443. [CrossRef] [PubMed]
30. Henriques, P.C.; Borges, I.; Pinto, A.M.; Magalhães, F.D.; Gonçalves, I.C. Fabrication and antimicrobial performance of surfaces integrating graphene-based materials. *Carbon* **2018**, *132*, 709–732. [CrossRef]
31. Dadi, R.; Azouani, R.; Traore, M.; Mielcarek, C.; Kanaev, A. Antibacterial activity of ZnO and CuO nanoparticles against gram positive and gram negative strains. *Mater. Sci. Eng. C* **2019**, *104*, 109968. [CrossRef] [PubMed]
32. Hasan, M.T.; Gonzalez, R.; Munoz, A.A.; Materon, L.; Parsons, J.G.; Alcoutlabi, M. Forcespun polyvinylpyrrolidone/copper and polyethylene oxide/copper composite fibers and their use as antibacterial agents. *J. Appl. Polym. Sci.* **2022**, *139*, 51773. [CrossRef]
33. Hasan, M.T.; Gonzalez, R.; Chipara, M.; Materon, L.; Parsons, J.; Alcoutlabi, M. Antibacterial activities of centrifugally spun polyethylene oxide/silver composite nanofibers. *Polym. Adv. Technol.* **2021**, *32*, 2327–2338. [CrossRef]
34. De la Garza, D.; De Santiago, F.; Materon, L.; Chipara, M.; Alcoutlabi, M. Fabrication and characterization of centrifugally spun poly(acrylic acid) nanofibers. *J. Appl. Polym. Sci.* **2019**, *136*, 47480. [CrossRef]
35. Smijs, T.G.; Pavel, S. Titanium dioxide and zinc oxide nanoparticles in sunscreens: Focus on their safety and effectiveness. *Nanotechnol. Sci. Appl.* **2011**, *4*, 95–112. [CrossRef] [PubMed]
36. Fortunato, E.; Gonçalves, A.; Pimentel, A.; Barquinha, P.; Gonçalves, G.; Pereira, L.; Ferreira, I.; Martins, R. Zinc oxide, a multifunctional material: From material to device applications. *Appl. Phys. A* **2009**, *96*, 197–205. [CrossRef]
37. Espitia, P.J.P.; Soares, N.d.F.F.; Coimbra, J.S.d.R.; de Andrade, N.J.; Cruz, R.S.; Medeiros, E.A.A. Zinc oxide nanoparticles: Synthesis, antimicrobial activity and food packaging applications. *Food Bioprocess Technol.* **2012**, *5*, 1447–1464. [CrossRef]
38. Franco, D.; Calabrese, G.; Guglielmino, S.P.P.; Conoci, S. Metal-Based Nanoparticles: Antibacterial Mechanisms and Biomedical Application. *Microorganisms* **2022**, *10*, 1778. [CrossRef] [PubMed]
39. Anedda, E.; Farrell, M.L.; Morris, D.; Burgess, C.M. Evaluating the impact of heavy metals on antimicrobial resistance in the primary food production environment: A scoping review. *Environ. Pollut.* **2023**, *320*, 121035. [CrossRef]
40. Kadiyala, U.; Kotov, N.A.; VanEpps, J.S. Antibacterial Metal Oxide Nanoparticles: Challenges in Interpreting the Literature. *Curr. Pharm. Des.* **2018**, *24*, 896–903. [CrossRef]
41. Du, J.; Tang, J.H.; Xu, S.D.; Ge, J.Y.; Dong, Y.W.; Li, H.X.; Jin, M.Q. ZnO nanoparticles: Recent advances in ecotoxicity and risk assessment. *Drug Chem. Toxicol.* **2020**, *43*, 322–333. [CrossRef] [PubMed]
42. Raha, S.; Ahmaruzzaman, M. ZnO nanostructured materials and their potential applications: Progress, challenges and perspectives. *Nanoscale Adv.* **2022**, *4*, 1868–1925. [CrossRef] [PubMed]
43. Rihova, M.; Cihalova, K.; Pouzar, M.; Kuthanova, M.; Jelinek, L.; Hromadko, L.; Cicmancova, V.; Heger, Z.; Macak, J.M. Biopolymeric fibers prepared by centrifugal spinning blended with ZnO nanoparticles for the treatment of Acne vulgaris. *Appl. Mater. Today* **2024**, *37*, 102151. [CrossRef]

44. Mohd Yusof, H.; Abdul Rahman, N.A.; Mohamad, R.; Hasanah Zaidan, U.; Samsudin, A.A. Antibacterial Potential of Biosynthesized Zinc Oxide Nanoparticles against Poultry-Associated Foodborne Pathogens: An In Vitro Study. *Animals* **2021**, *11*, 2093. [CrossRef] [PubMed]
45. Mendes, C.R.; Dilarri, G.; Forsan, C.F.; Sapata, V.d.M.R.; Lopes, P.R.M.; de Moraes, P.B.; Montagnolli, R.N.; Ferreira, H.; Bidoia, E.D. Antibacterial action and target mechanisms of zinc oxide nanoparticles against bacterial pathogens. *Sci. Rep.* **2022**, *12*, 2658. [CrossRef] [PubMed]
46. Zhou, X.; Shi, T.; Zhou, H. Hydrothermal preparation of ZnO-reduced graphene oxide hybrid with high performance in photocatalytic degradation. *Appl. Surf. Sci.* **2012**, *258*, 6204–6211. [CrossRef]
47. Kumar, P.; Som, S.; Pandey, M.K.; Das, S.; Chanda, A.; Singh, J. Investigations on optical properties of ZnO decorated graphene oxide (ZnO@GO) and reduced graphene oxide (ZnO@r-GO). *J. Alloys Compd.* **2018**, *744*, 64–74. [CrossRef]
48. Chung, K.; Lee, C.-H.; Yi, G.-C. Transferable GaN Layers Grown on ZnO-Coated Graphene Layers for Optoelectronic Devices. *Science* **2010**, *330*, 655–657. [CrossRef] [PubMed]
49. Lee, J.M.; Pyun, Y.B.; Yi, J.; Choung, J.W.; Park, W.I. ZnO Nanorod−Graphene Hybrid Architectures for Multifunctional Conductors. *J. Phys. Chem. C* **2009**, *113*, 19134–19138. [CrossRef]
50. Mao, J.; Li, J.J.; Ling, T.; Liu, H.; Yang, J.; Du, X.W. Facile synthesis of zinc hydroxide carbonate flowers on zinc oxide nanorods with attractive luminescent and optochemical performance. *Nanotechnology* **2011**, *22*, 245607. [CrossRef]
51. Du, Y.Q.; Li, G.Y.; Ye, L.; Che, C.J.; Yang, X.H.; Zhao, L.J. Sandwich-like Ni-Zn hydroxide nanosheets vertically aligned on reduced graphene oxide via MOF templates towards boosting supercapacitive performance. *Chem. Eng. J.* **2021**, *417*, 129189. [CrossRef]
52. Nabipour, H.; Sadr, M.H.; Thomas, N. Synthesis, characterisation and sustained release properties of layered zinc hydroxide intercalated with amoxicillin trihydrate. *J. Exp. Nanosci.* **2015**, *10*, 1269–1284. [CrossRef]
53. Flores, K.; Valdes, C.; Ramirez, D.; Eubanks, T.M.; Lopez, J.; Hernandez, C.; Alcoutlabi, M.; Parsons, J.G. The effect of hybrid zinc oxide/graphene oxide (ZnO/GO) nano-catalysts on the photocatalytic degradation of simazine. *Chemosphere* **2020**, *259*, 127414. [CrossRef] [PubMed]
54. Kumar, P.; Penta, S.; Mahapatra, S.P. Dielectric Properties of Graphene Oxide Synthesized by Modified Hummers' Method from Graphite Powder. *Integr. Ferroelectr.* **2019**, *202*, 41–51. [CrossRef]
55. Shahriary, L.; Athawale, A.A. Graphene oxide synthesized by using modified hummers approach. *Int. J. Renew. Energy Environ. Eng.* **2014**, *2*, 58–63.
56. Sun, H.J.; Yang, Y.H.; Huang, Q. Preparation and Structural Variation of Graphite Oxide and Graphene Oxide. *Integr. Ferroelectr.* **2011**, *128*, 163–170. [CrossRef]
57. Lee, D.W.; De Los Santos, L.; Seo, J.W.; Felix, L.L.; Bustamante, A.; Cole, J.M.; Barnes, C.H.W. The Structure of Graphite Oxide: Investigation of Its Surface Chemical Groups. *J. Phys. Chem. B* **2010**, *114*, 5723–5728. [CrossRef] [PubMed]
58. Wang, H.; Hu, Y.H. Effect of Oxygen Content on Structures of Graphite Oxides. *Ind. Eng. Chem. Res.* **2011**, *50*, 6132–6137. [CrossRef]
59. Morales, H.M.; Vieyra, H.; Sanchez, D.A.; Fletes, E.M.; Odlyzko, M.; Lodge, T.P.; Padilla-Gainza, V.; Alcoutlabi, M.; Parsons, J.G. Synthesis and Characterization of Titanium Nitride–Carbon Composites and Their Use in Lithium-Ion Batteries. *Nanomaterials* **2024**, *14*, 624. [CrossRef]
60. Gordeeva, A.; Hsu, Y.-J.; Jenei, I.Z.; Brant Carvalho, P.H.B.; Simak, S.I.; Andersson, O.; Häussermann, U. Layered Zinc Hydroxide Dihydrate, $Zn_5(OH)_{10}\cdot 2H_2O$, from Hydrothermal Conversion of ε-$Zn(OH)_2$ at Gigapascal Pressures and its Transformation to Nanocrystalline ZnO. *ACS Omega* **2020**, *5*, 17617–17627. [CrossRef]
61. Botez, C.E.; Morris, J.L.; Manriquez, A.J.E.; Anchondo, A. Heating induced structural and chemical behavior of KDPO in the 25 °C–215 °C temperature range. *Mater. Charact.* **2013**, *83*, 74–78. [CrossRef]
62. Morales, H.M.; Vieyra, H.; Sanchez, D.A.; Fletes, E.M.; Odlyzko, M.; Lodge, T.P.; Padilla-Gainza, V.; Alcoutlabi, M.; Parsons, J.G. Synthesis and Characterization of Vanadium Nitride/Carbon Nanocomposites. *Int. J. Mol. Sci.* **2024**, *25*, 6952. [CrossRef] [PubMed]
63. Rani, J.R.; Lim, J.; Oh, J.; Kim, D.; Lee, D.; Kim, J.-W.; Shin, H.S.; Kim, J.H.; Jun, S.C. Substrate and buffer layer effect on the structural and optical properties of graphene oxide thin films. *RSC Adv.* **2013**, *3*, 5926–5936. [CrossRef]
64. Gupta, B.; Kumar, N.; Panda, K.; Kanan, V.; Joshi, S.; Visoly-Fisher, I. Role of oxygen functional groups in reduced graphene oxide for lubrication. *Sci. Rep.* **2017**, *7*, 45030. [CrossRef] [PubMed]
65. Al-Gaashani, R.; Najjar, A.; Zakaria, Y.; Mansour, S.; Atieh, M.A. XPS and structural studies of high quality graphene oxide and reduced graphene oxide prepared by different chemical oxidation methods. *Ceram. Int.* **2019**, *45*, 14439–14448. [CrossRef]
66. Jnido, G.; Ohms, G.; Viöl, W. Deposition of zinc oxide coatings on wood surfaces using the solution precursor plasma spraying process. *Coatings* **2021**, *11*, 183. [CrossRef]
67. Lin, B.C.; Shen, P.; Chen, S.Y. ZnO and epsilon-Zn(OH)(2) Composite Nanoparticles by Pulsed Laser Ablation on Zn in Water. *J. Phys. Chem. C* **2011**, *115*, 5003–5010. [CrossRef]
68. Wang, M.S.; Jiang, L.X.; Kim, E.J.; Hahn, S.H. Electronic structure and optical properties of Zn(OH)(2): LDA+U calculations and intense yellow luminescence. *RSC Adv.* **2015**, *5*, 87496–87503. [CrossRef]
69. Sitko, R.; Turek, E.; Zawisza, B.; Malicka, E.; Talik, E.; Heimann, J.; Gagor, A.; Feist, B.; Wrzalik, R. Adsorption of divalent metal ions from aqueous solutions using graphene oxide. *Dalton Trans.* **2013**, *42*, 5682–5689. [CrossRef]

70. Kasaeian, M.; Ghasemi, E.; Ramezanzadeh, B.; Mahdavian, M.; Bahlakeh, G. A combined experimental and electronic-structure quantum mechanics approach for studying the kinetics and adsorption characteristics of zinc nitrate hexahydrate corrosion inhibitor on the graphene oxide nanosheets. *Appl. Surf. Sci.* **2018**, *462*, 963–979. [CrossRef]
71. Seredych, M.; Mabayoje, O.; Kolesnik, M.M.; Krstic, V.; Bandosz, T.J. Zinc (hydr)oxide/graphite based-phase composites: Effect of the carbonaceous phase on surface properties and enhancement in electrical conductivity. *J. Mater. Chem.* **2012**, *22*, 7970–7978. [CrossRef]
72. Kumar, A.; Joseph, S.; Tsechansky, L.; Privat, K.; Schreiter, I.J.; Schüth, C.; Graber, E.R. Biochar aging in contaminated soil promotes Zn immobilization due to changes in biochar surface structural and chemical properties. *Sci. Total Environ.* **2018**, *626*, 953–961. [CrossRef] [PubMed]
73. Mandal, P.; Ghosh, S.K.; Grewal, H.S. Graphene oxide coated aluminium as an efficient antibacterial surface. *Environ. Technol. Innov.* **2022**, *28*, 102591. [CrossRef]
74. Menazea, A.A.; Ahmed, M.K. Synthesis and antibacterial activity of graphene oxide decorated by silver and copper oxide nanoparticles. *J. Mol. Struct.* **2020**, *1218*, 128536. [CrossRef]
75. Emami-Karvani, Z.; Chehrazi, P. Antibacterial activity of ZnO nanoparticle on gram-positive and gram-negative bacteria. *Afr. J. Microbiol. Res.* **2011**, *5*, 1368–1373.
76. Jones, N.; Ray, B.; Ranjit, K.T.; Manna, A.C. Antibacterial activity of ZnO nanoparticle suspensions on a broad spectrum of microorganisms. *FEMS Microbiol. Lett.* **2008**, *279*, 71–76. [CrossRef] [PubMed]
77. Bouttier-Figueroa, D.C.; Garcia-Valenzuela, J.A.; Cabrera-German, D.; Cota-Leal, M.; Quevedo-Lopez, M.A.; Rosas-Durazo, A.; Sotelo-Lerma, M. Characterization of the antibacterial galactomannan/Zn(OH)(2)-ZnO composite material prepared from a green process using mesquite seeds as a biopolymer source. *Bull. Mater. Sci.* **2019**, *42*, 116. [CrossRef]
78. Khafri, H.Z.; Ghaedi, M.; Asfaram, A.; Javadian, H.; Safarpoor, M. Synthesis of CuS and ZnO/Zn(OH)(2) nanoparticles and their evaluation for in vitro antibacterial and antifungal activities. *Appl. Organomet. Chem.* **2018**, *32*, e4398. [CrossRef]
79. Haque, S.; Faidah, H.; Ashgar, S.S.; Abujamel, T.S.; Mokhtar, J.A.; Almuhayawi, M.S.; Harakeh, S.; Singh, R.; Srivastava, N.; Gupta, V.K. Green Synthesis of Zn(OH)(2)/ZnO-Based Bionanocomposite using Pomegranate Peels and Its Application in the Degradation of Bacterial Biofilm. *Nanomaterials* **2022**, *12*, 3458. [CrossRef]
80. Awassa, J.; Soule, S.; Cornu, D.; Ruby, C.; El-Kirat-Chatel, S. Understanding the role of surface interactions in the antibacterial activity of layered double hydroxide nanoparticles by atomic force microscopy. *Nanoscale* **2022**, *14*, 10335–10348. [CrossRef]
81. Tariq, M.; Khan, A.U.; Rehman, A.U.; Ullah, S.; Jan, A.U.; Zakareya; Khan, Z.U.; Muhammad, N.; Ul Islam, Z.; Yuan, Q.P. Green synthesis of Zno@GO nanocomposite and its' efficient antibacterial activity. *Photodiagn. Photodyn. Ther.* **2021**, *35*, 102471. [CrossRef] [PubMed]
82. Hsueh, Y.H.; Hsieh, C.T.; Chiu, S.T.; Tsai, P.H.; Liu, C.Y.; Ke, W.J. Antibacterial Property of Composites of Reduced Graphene Oxide with Nano-Silver and Zinc Oxide Nanoparticles Synthesized Using a Microwave-Assisted Approach. *Int. J. Mol. Sci.* **2019**, *20*, 5394. [CrossRef] [PubMed]
83. Sahin, E.; Musevi, S.J.; Aslani, A. Antibacterial activity against and characterization of ZnO and ZnO-AlO mixed oxide nanoparticles. *Arab. J. Chem.* **2017**, *10*, S230–S235. [CrossRef]
84. Ahmadi, R.; Nafchi, R.F.; Sangpour, P.; Bagheri, M.; Badiei, E. A comparative study: Green synthesis and evaluation of ZnO-GO and ZnO-RGO nanocomposites for antibacterial applications. *Mater. Sci. Eng. B Adv.* **2023**, *294*, 116555. [CrossRef]
85. Prasad, K.; Lekshmi, G.S.; Ostrikov, K.; Lussini, V.; Blinco, J.; Mohandas, M.; Vasilev, K.; Bottle, S.; Bazaka, K.; Ostrikov, K. Synergic bactericidal effects of reduced graphene oxide and silver nanoparticles against Gram-positive and Gram-negative bacteria. *Sci. Rep.* **2017**, *7*, 1591. [CrossRef]
86. Karaky, N.; Tang, S.Y.; Ramalingam, P.; Kirby, A.; McBain, A.J.; Banks, C.E.; Whitehead, K.A. Multidrug-Resistant Remains Susceptible to Metal Ions and Graphene-Based Compounds. *Antibiotics* **2024**, *13*, 381. [CrossRef]